Self-assembly of fully addressable DNA nanostructures from double crossover tiles

Wen Wang[1,2,3], Tong Lin[1], Suoyu Zhang[1], Tanxi Bai[1], Yongli Mi[2,3,4,*] and Bryan Wei[1,*]

[1]School of Life Sciences, Tsinghua University-Peking University Center for Life Sciences, Center for Synthetic and Systems Biology, Tsinghua University, Beijing 100084, China, [2]Bioengineering Graduate Program, The Hong Kong University of Science and Technology, Clear Water Bay, Kowloon, Hong Kong, [3]Depatment of Chemistry, Tongji University, Shanghai 200092, China and [4]Department of Chemical and Biomolecular Engineering, The Hong Kong University of Science and Technology, Clear Water Bay, Kowloon, Hong Kong

ABSTRACT

DNA origami and single-stranded tile (SST) are two proven approaches to self-assemble finite-size complex DNA nanostructures. The construction elements appeared in structures from these two methods can also be found in multi-stranded DNA tiles such as double crossover tiles. Here we report the design and observation of four types of finite-size lattices with four different double crossover tiles, respectively, which, we believe, in terms of both complexity and robustness, will be rival to DNA origami and SST structures.

INTRODUCTION

Two recently developed approaches in DNA self-assembly, DNA origami (1–11) and single-stranded tile (SST) (12–15), are capable of producing finite-size mega-Dalton structures by encoding programmable DNA complementarity. In DNA origami approach, a long scaffold (e.g. M13 viral genome) is folded, by hundreds of short synthetic strands with distinct sequences, into a complex structure. More recently, SSTs, uniquely sequenced short synthetic strands serving as tiles, are designed to self-assemble into finite-size 2-dimensional (2-D) and 3-dimensional (3-D) shapes with comparable complexity to that of DNA origami structures.

Tracing back to the earlier development in the DNA nanotechnology, there reveals that similar structural elements appeared in DNA origami and SST structures can also be found in those self-assembled from multi-stranded tiles, including junction tiles (16–31), planar tiles (31–42) and other tiles (43–58). Among a vast collection of tiles that have been developed, double crossover (DX) tile (32,33) was the first rigid tile introduced to the field. It was one of the early milestones in the field that successfully showed the feasibility of using rigid tile to build 2-D lattice.

Inspired by the successful formation of complex structures from DNA origami and SST, the question we want to ask here is whether we can use the multi-stranded rigid tiles (e.g. DX tiles) to build finite-size structures with similar complexity to that of DNA origami or SST based structures. In this study, we have designed finite-size lattices with different DX tiles. Four species of DX tiles were used to construct four different types of finite-size lattices respectively. One of four types was also constructed hierarchically in two consecutive steps, with the first step to form individual tiles separately and the second step to form the desired lattice from the mixture of individual tiles. Furthermore, a larger lattice with more component tiles and the corresponding patterns were built. Lastly, infinite-size AB stripe lattices were formed with unpurified DNA strands.

MATERIALS AND METHODS

DNA sequence design

DNA sequences were designed with the UNIQUIMER software (59) to meet the following rules: (i) nucleotides (that is, A, C, G and T) are randomly generated one by one along each oligonucleotide chain. (ii) Complementary nucleotides to ones generated in (i) are matched following the base-pairing rule: A to T and vice versa; C to G and *vice versa*. (iii) No repeating segment beyond a certain length (seven or eight nucleotides) is allowed. When such repeating segments appear during design, the most recently generated nucleotides will be mutated until the repeating-segment requirement is satisfied. (iv) No four consecutive A, C, G or T bases are allowed. Poly(T) domains were manually designed and concatenated to certain strands. DNA strands were synthesized by Integrated DNA Technology, Inc. (www.idtdna.com) or Bioneer Corporation (www.bioneer.com).

*To whom correspondence should be addressed. Tel: +86 10 62788746; Fax: +86 10 62788746; Email: bw@tsinghua.edu.cn
Correspondence may also be addressed to Yongli Mi. Tel: +852 23587127; Fax: +852 23580004; Email: keymix@ust.hk

Sample preparation

To assemble the structures, DNA strands were mixed, to a roughly equal molar final concentration of 100 nM for all the structures except the patterns based on the 9 × 10 lattice (90 nM) and the infinite-size lattices (1000 nM), in 0.5× TE buffer (5 mM Tris, pH = 7.9, 1 mM ethylenediaminetetraacetic acid) supplemented with 15 mM MgCl₂. We note that the DNA concentrations were based on the manufacturer's specifications and that no additional in-house calibration was performed. Thus, the stoichiometry for the strands was not carefully adjusted. The DNA mixture was then annealed in either a 'ramp' annealing program cooling from 90 to 25°C (or 10°C) over a period of 17–76 h or under the isothermal incubation at a fixed temperature (e.g. 60°C) for 3 h after a 5 min denaturing treatment at 90°C (see Supplementary Section 2.1, 4.2, 5.1, 5.5 and 6.1 for detailed annealing protocols).

The annealed samples were subjected to 1 or 2% native agarose gel electrophoresis in an ice-water bath, and the gel was prepared in 0.5× TBE (44.5 mM Tris, pH =8.3, 44.5 mM boricacid, 1 mM ethylenediaminetetraacetic acid) buffer supplemented with 10 mM MgCl₂ and pre-stained with SYBR Safe. Then the target gel bands were excised, finely crushed using a microtube pestle, in a Freeze 'N Squeeze column (Bio-Rad), and then directly subjected to centrifugation at 438 *g* for 3 min at 4°C. Samples centrifuged through the column were collected for concentration estimation by the measurement of ultraviolet absorption at 260 nm. Such estimation is useful for estimating the dilution factor before atomic force microscopy (AFM).

Structure stabilization by ligation

For some fragile structures (e.g. 6 × 5 lattices with DX tiles III or IV), ligation was used to seal nicks in the assembled structures to improve structural stability (60,61). T4 DNA ligase seals nicks by catalyzing the formation of a covalent phosphodiester bond between the 5′ phosphate of one DNA strand and the 3′ hydroxyl of another across the nicking point. The 5′ phosphate is typically not available in synthetic DNA, but can be added by T4 Polynucleotide Kinase (PNK). DNA mixture (100 nM per strand) was incubated with PNK in 1× DNA ligase buffer (40 mM Tris–HCl, pH = 7.8, 10 mM MgCl₂, 10 mM Dithiothreitol (DTT), 10 mM adenosine triphosphate (ATP)) at 37°C for 5 h to get all DNA strands 5′ phosphorylated. After annealing for structural self-assembly, T4 DNA ligase (4 × 10⁶ units/nM DNA) was directly added to the DNA mixture and incubated at 16°C for at 16 h.

For samples in two-step annealing, they were treated with PNK after annealing. A 20-μl annealed sample was incubated with 0.8 μl PNK (10 000U/ml) in 1× DNA ligase buffer (40mM Tris–HCl, pH = 7.8, 10 mM DTT, 10 mM ATP) at 37°C for 4 h. After phosphorylation, 0.4 μl T4 DNA ligase (400 000U/ml) was directly added to the mixture with an incubation at 37°C for 1 h.

AFM imaging

AFM images were obtained using an SPM Multimode with Nanoscope V controller (Bruker Corp.). A 5-μl droplet (2–10 nM) of purified sample (annealed sample without purification for the infinite-size lattice) and then a 40 μl drop of 0.5× TE buffer (10 mM MgCl₂) were applied to a freshly cleaved mica surface and left for ∼2 min. Supplementary 10 μl 10mM NiCl₂ was added to increase the strength of DNA–mica binding (62). NiCl₂ supplementation was skipped when imaging 9 × 10 DX lattice without a quality downgrade under AFM. To image the pattern 'T', 1 μl streptavidin (0.5 mg/ml in 0.5× TE buffer) was added to the sample droplet on mica for 2 min before imaging. Additional dilution of the sample was performed sometimes to achieve the desired sample density. Samples were imaged under liquid ScanAsyst mode, with C-type triangular tips (resonant frequency, $f_0 = 40$–75 kHz; spring constant, $k = 0.24$ N m^{-1}) from the SNL-10 silicon nitride cantilever chip (Bruker Corp.).

Yield quantification by gel electrophoresis

Yield was estimated by analysis under native agarose gel electrophoresis, pre-stained with SYBR Safe DNA stain. The intensity of the target band was compared against a standard band (12) (e.g. 1500-base-pair band from a 1-kb DNA ladder mixture). The mass value of the target band was deduced from the intensity–mass correlation based on the standard band, and was used to calculate the yield of the desired structure.

Measurement and statistics

AFM measurements were obtained using the section function of NANOSCOPE ANALYSIS (version 1.50; Bruker Corp.). About 35–72 sample points were collected from AFM images of each individual DX tile for each distance measurement and statistics (i.e. length and width of each individual tile). The mean value and standard deviation were calculated for four types of DX tiles (Supplementary Section 2.4).

Annealing curve and corresponding analysis

SYBR Green I was added to annealing sample and fluorescence intensity was recorded by a real-time polymerase chain reaction thermal cycler through the cooling from 90 to 25°C. The derivative of the fluorescence with respect to temperature was obtained by subtracting two fluorescent intensities obtained one degree apart (63,64).

RESULTS

Designs of complex nanostructures with DX tiles

We used double crossover-antiparallel-even spacing (DAE) tile (32,33), the most widely used DX tile type, in this study. The antiparallel DX tile can be viewed as two juxtaposed immobile Holliday junctions at which the two non-crossover strands are antiparallel to each other (Figure 1A, strands 1 and 5). As the design of intra-tile base pairing depicts, five constituent strands form a DX tile with four single-stranded sticky ends and a rigidity core of two double-stranded helices bundled by two crossovers (Figure 1A). The sticky ends at both sides could be programmed
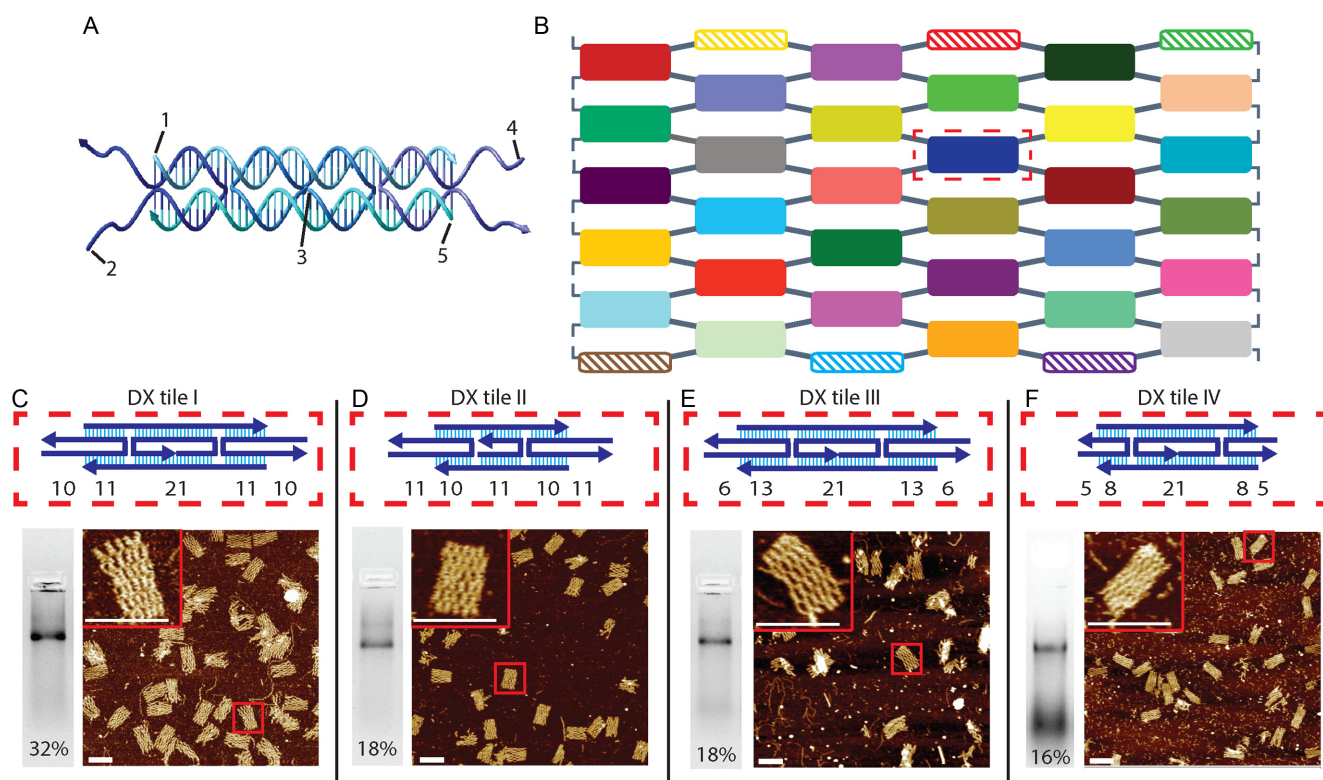
Figure 1. Design and self-assembly of four types of 6 × 5 lattices with DX tiles I, II, III and IV. (**A**) 3D model of a DX tile (strand numbers as shown). (**B**) Schematic diagram of a 6 × 5 lattice. Solid rectangles depict common DX tiles and shaded rectangles depict stitch tiles (strand diagrams in Supplementary Figure S1). (**C–F**). Self-assembly of 6 × 5 lattices with DX tiles I (C), II (D), III (E) and IV (F) respectively. Top: strand diagram of a DX tile; bottom left: native agarose gel electrophoresis result of annealed sample (number indicates yield; yield quantification in Supplementary Section 2.2); bottom right: AFM image of annealed sample after gel purification with inset showing a magnified view (scale bars: 100 nm). Note that AFM images in (E) and (F) were taken after ligation treatment for structural stabilization and those without treatment are shown in Supplementary Figures S7b and 8b.

for DX tiles to pair up with desired neighbors to form prescribed global shape.

As shown in Figure 1B, we assembled a 6 × 5 lattice with 30 distinct DX tiles, each of which consists of five strands. In order to prevent from blunt end stacking and undesirable base paring, we replaced the sequences of unpaired sticky ends at the vertical boundary positions with poly(T) (multiple thymine bases). For each 6 × 5 lattice, we also designed six stitch tiles to fill in the gaps between two neighboring DX tiles at horizontal boundaries to maintain structural integrity (shaded rectangles in Figure 1B and detailed strand diagrams in Supplementary Figure S1). Four species of DX tiles were designed as shown in Figure 1C–F and they differ in spacing between two crossover points (two helical turns for DX tiles I, III and IV, and one turn for DX tile II) and length of sticky ends (DX tile I: 10 nt, DX tile II: 11 nt, DX tile III: 6 nt and DX tile IV: 5 nt). With shorter sticky ends in tiles III and IV, they are expected to have weaker inter-tile base pairing strength, compared to that of tiles I and II (see details in Supplementary Sections 2 and 3).

DX tiles I, II, III and IV were designed to self-assemble into four types of 6 × 5 lattices respectively (Figure 1C–F). To show the scalability of the method, a larger 9 × 10 lattice was also designed with DX tile I. A unique DNA sequence was appointed to each component strand of a certain lattice and sequences were generated using software UNIQUIMER (59) (Sequence information can be found in Supplementary 2).

One-pot self-assembly

Four types of 6 × 5 lattices were constructed using unpurified DNA strands without strict stoichiometry adjustment. For each structure, after single-step (one-pot) annealing from 90 to 25°C (or 10°C) overnight in 0.5× TE buffer supplemented with 15 mM Mg^{2+}, the solution was subjected to 2% native agarose gel electrophoresis, which demonstrates a dominant band (Figure 1C–F, left panels; yield quantification in Supplementary Figure S2 and Table S1). The product in the target band was then extracted and purified by centrifugation. The purified samples were characterized using AFM. A rectangular morphology with desired number of DX tiles and dimensions was observed (Figure 1C–F and Supplementary Figures S3–6). Note that fragmented structures, especially for the lattices with DX tiles III and IV (shorter sticky ends), were observed under AFM (Supplementary Figures S7b and 8b), indicating a certain degree of fragility of the resulted structures.

Structure stabilization by ligation

Weak inter-tile binding of DX tiles III or IV would be resulted from a shorter sticky end pairing (six or five base-pair

duplex flanked by a pair of nicks), but sealing of the nicks is expected to substantially improve the mechanical stability of the resulted structures (60,61). In this study, the samples were treated with T4 DNA ligase with a pre-processing of phosphorylation at 5' terminals either before or after annealing. After such a treatment, mechanical strength of the lattices with DX tile III or IV was greatly improved. Under the AFM observation, well-formed lattices (with more than 95% of component tiles) in the ligated samples (Figure 1E and F) were significantly more than those in the samples without ligation (see detailed comparison between the results with and without ligation treatment in Supplementary Sections 3.2 and 4.5).

For DX tiles I, III and IV, there is also a nick inside the rigidity core (c.f. Figure 1A, strand 3) subjected to ligation reaction, which, however, is not as critical as the nick sealing across the paired sticky ends for structural reinforcement.

Hierarchical self-assembly

Real-time fluorometric measurement, a commonly adopted method in the field, was used to monitor the assembly rate over the annealing temperature range to reveal the critical temperature(s) of structure formation (63,64). Annealing curves and corresponding analysis were demonstrated in a case study of the 6×5 lattice formation with DX tile III.

Considering that the lengths of the intra-tile binding are longer than those of the sticky ends (Figure 1E), our original hypothesis about DX tile III was that individual tiles would form at a relatively higher temperature and the successive lattice formation would happen at a relatively lower temperature. Consequently, we had expected to observe multiple peaks in the annealing curve analysis, with the higher transition temperature(s) corresponding to the tile formation from component strands and the lowest transition temperature corresponding to the successive lattice formation from the pre-formed tiles. Surprisingly, we found that the peak pattern in the annealing curve of overall structure formation was similar to those of the corresponding individual component tiles (Supplementary Figure S9), which suggests that lattice formation happen almost right after individual tile formation.

Based on these results from the analysis, the lattice with DX tile III was constructed under isothermal annealing conditions. We found that 60°C was the temperature with the highest yield (Supplementary Figure S11), which is consistent with results from the annealing curve analysis.

We also tried the annealing curve analysis for the formation of lattices with DX tiles I, II and IV respectively. Single transition peak for DX tiles I and II was found respectively at 65 and 50°C (Supplementary Figure S10a and b). Dual transition peaks were found at around 50 and 65°C for DX tile IV, while similar pattern of dual transition peaks was also found in the annealing curve of individual DX tile IV (Supplementary Figure S10c). For all four types of 6×5 lattices, no additional peak associated with inter-tile binding was observed in the annealing curves, compared to the annealing curves of corresponding individual tiles (or mixture of tiles without inter-tile binding).

Although there is no obvious sequential order of hierarchies in the formation of the 6×5 DX lattices during
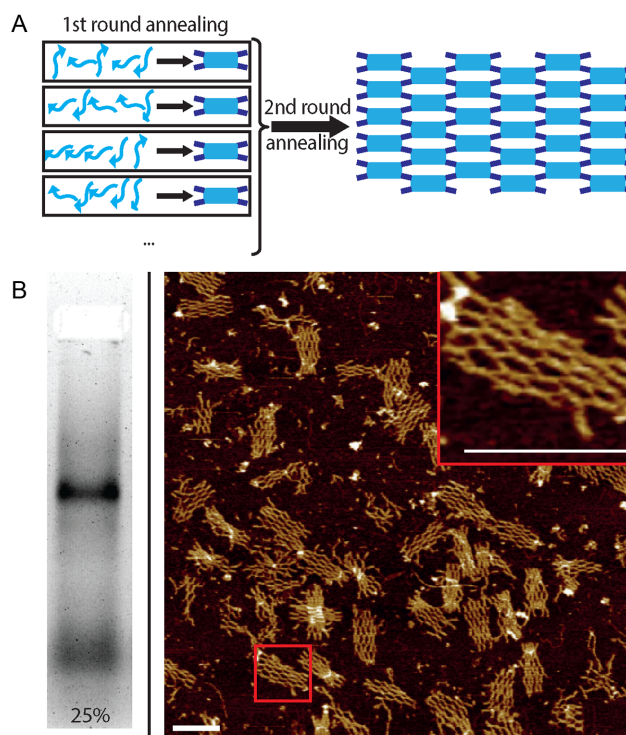

Figure 2. Hierarchical self-assembly of 6×5 lattice with DX tile I. (**A**) Schematic diagram of hierarchical assembly. (**B**) Native agarose gel electrophoresis result of annealed sample without ligation treatment (left) and AFM image (right) of annealed sample with ligation treatment after gel purification with inset showing a magnified view (scale bars: 100 nm). AFM image of annealed sample without ligation treatment is shown in Supplementary Figure S14b.

the one-pot annealing, the hierarchies could be generated manually by splitting the self-assembly into two consecutive steps as illustrated in Figure 2A. In the first step, component strands were mixed and annealed to form each DX tile individually and the formation of individual tiles was confirmed by native agarose gel electrophoresis (Supplementary Figure S12). In the second step, individual tiles formed in the first step were mixed for a second round of annealing under the isothermal conditions to form the desired lattice. The annealed sample after the second step was subjected to native agarose gel electrophoresis (Figure 2B, left panel; Supplementary Figure S13) and AFM imaging (Figure 2B, right panel), and the results demonstrate the successful formation of the desired structures after the two-step annealing.

Self-assembly of a larger DX lattice and the corresponding patterns

Encouraged by the successful self-assemblies of 6×5 DX lattices, we further designed a 9×10 DX lattice with DX tile I (Figure 3A). This lattice, containing 90 DX tiles, is 1.5 times as large as a common origami structure. The strand mixture was annealed from 90 to 25°C over 76 h in 0.5× TE buffer supplemented with 15 mM Mg^{2+} to form the desired structure. The successful self-assembly was verified by native agarose gel electrophoresis and AFM imaging (Fig-
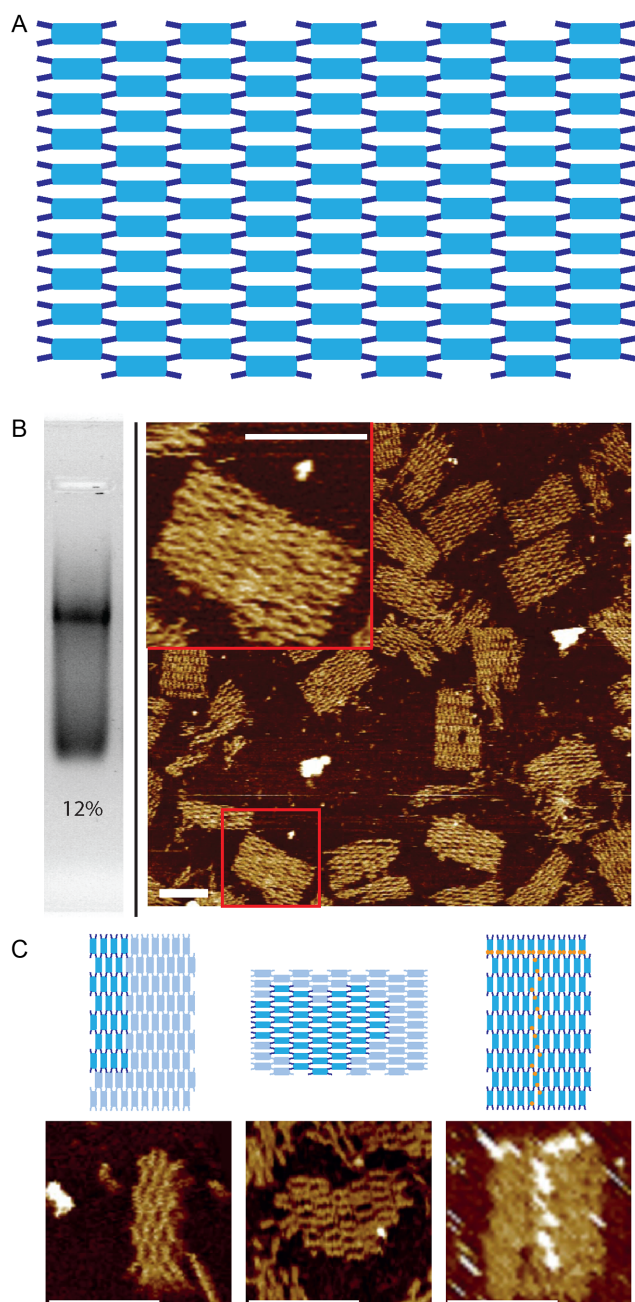
Figure 4. The Infinite-size DX lattice. (**A**) Lattice schematics. (**B**) AFM results. Inset: a magnified view (scale bars: 100 nm).

Figure 3. 9 × 10 DX lattice and the corresponding patterns. (**A**) 9 × 10 DX lattice schematics. (**B**) Native agarose gel electrophoresis and AFM results of the 9 × 10 DX lattice. Left: gel result (number indicates yield, C.F. Supplementary Figure S15); right: AFM image of annealed sample after gel purification with inset showing a magnified view. (**C**) Patterns 'I', heart and 'T' based on 9 × 10 DX lattice (c.f. Supplementary Figure S17). Top: schematics; bottom: AFM images of patterns. Scale bars: 100 nm.

ure 3B). Because the 9 × 10 lattice is an apparent modular canvas to demonstrate different patterns when certain tiles are withheld or decorated. We designed two patterns by withholding subsets of component tiles with edge protectors to pair with single-stranded overhangs, and one pattern by decorating the chosen tiles with streptavidin (Figure 3C, top panels). After specified strands were annealed in a sim-
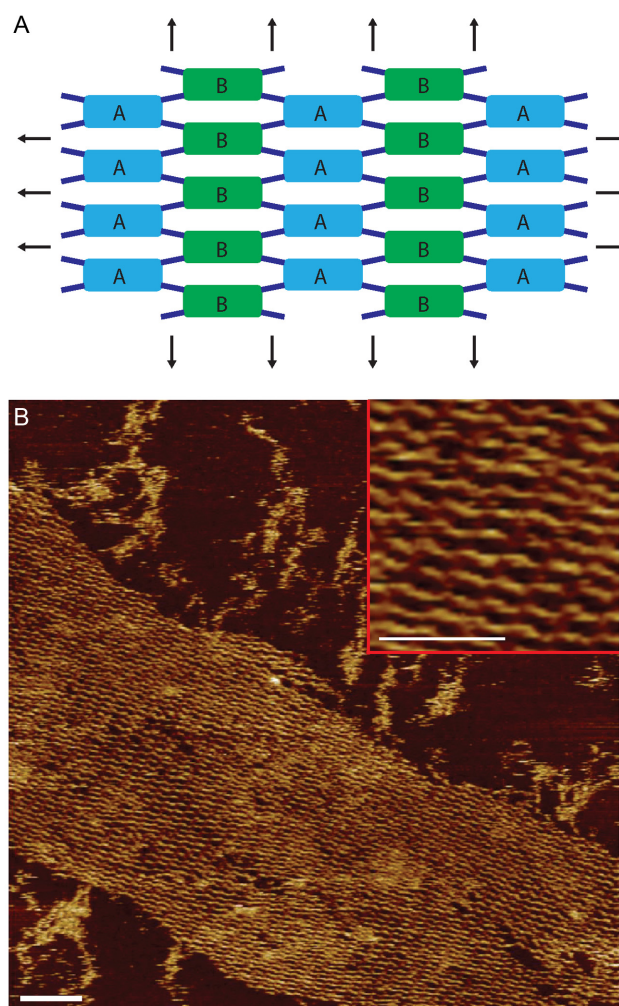
ilar condition to that of 9 × 10 lattice, we observed successful formation of the patterns on agarose gel electrophoresis (Supplementary Figure S18) and under AFM (Figure 3C, bottom panels, Supplementary Figures S16, S19–21).

Self-assembly of infinite-size lattices

Traditionally, purified DNA strands with careful adjustment of stoichiometry were used to self-assemble desired infinite-size structures in tiling approach. The successful formation of the complex finite size structures by unpurified strands in this study, as well as earlier investigations (12–15), inspired us to use unpurified strands in self-assembly of infinite-size lattices. Under similar conditions of the finite-size lattice formation, we constructed striped infinite-size lattices of the simplest two-tile (A and B) systems (Figure 4A), with the results comparable to the ones from the earlier studies (Figure 4B; Supplementary Figures S22 and 23) (33).

DISCUSSION

Multi-stranded tiles, such as DX tiles, have been developed since early 80s and the structures with different periodical nanoscale patterns have been reported (65–68). Although the size of the self-assembled structures can reach to micron or even millimeter size (29,41,45,69), the overall complexity of the structure from tiling approach is limited, which was also the case for finite-size structures based on multi-stranded tiles (21,23,44). In this study, we have demonstrated that multi-stranded tile (e.g. DX tile) based structures can reach a similar complexity level to that of DNA origami and SST based structures.

In SST system, simplest building blocks are adopted and extremely high resolution of addressability ($\sim 3 \times 7$ nm) is achieved. On the other hand, larger building blocks are presented in this multi-stranded tile (e.g. DX tile) system, so the resolution of addressability seems to be lower. However, because all component strands are distinctive to one another, the resolution of addressability for this DX system can be calculated down to the strand level from the tile level.

Unpurified strands were used in the structure formation throughout the study, which made the experiments easier and more cost effective. To our surprise, similar experimental arrangement can also be applied to form infinite-size DX lattices that used to be formed only by purified strands, although the defect rate of the resulted structures appeared to be higher than those from earlier studies in which purified strands with careful stoichiometry adjustment were adopted.

We have shown in this article that hierarchical assembly can be carried out by sequential formation of separate DX tiles from multiple strands and then the successive lattice formation from individual tiles, which shows higher assembly yield than that from one-pot annealing. However, in a slow cooling from 90 to 25°C, and sequential order of tile formation and successive lattice formation was not detectable in annealing curve analysis. It suggests that the lattice formation takes place right after the self-assembly of individual tiles in one-pot annealing.

In summary, we have reported a new self-assembly scheme of finite-size lattices with four species of DX tiles. Both one-pot and hierarchical annealing were carried out with comparable yields. Such a system complements origami and SST approaches for constructing complex structures. Besides DX tiles, we believe more multi-stranded tiles and other nanoscale objects (e.g. DNA origami units and nanoparticles) can be applied to form finite-size structures under a similar self-assembly principle (70). After the triumphant introductions of DNA origami and SST, this successful implementation of DX tiles in finite-size structures once again call for in-depth mechanistic investigations on complex systems of molecular self-assembly.

SUPPLEMENTARY DATA

Supplementary Data are available at NAR Online.

ACKNOWLEDGEMENTS

The authors thank Peng Yin for helpful discussions. W.W. acknowledges financial support from Chinese Ministry of

REFERENCES

1. Rothemund,P.W. (2006) Folding DNA to create nanoscale shapes and patterns. *Nature*, **440**, 297–302.
2. Andersen,E.S., Dong,M., Nielsen,M.M., Jahn,K., Subramani,R., Mamdouh,W., Golas,M.M., Sander,B., Stark,H., Oliveira,C.L. *et al.* (2009) Self-assembly of a nanoscale DNA box with a controllable lid. *Nature*, **459**, 73–76.
3. Dietz,H., Douglas,S.M. and Shih,W.M. (2009) Folding DNA into twisted and curved nanoscale shapes. *Science*, **325**, 725–730.
4. Douglas,S.M., Dietz,H., Liedl,T., Hogberg,B., Graf,F. and Shih,W.M. (2009) Self-assembly of DNA into nanoscale three-dimensional shapes. *Nature*, **459**, 414–418.
5. Ke,Y., Douglas,S.M., Liu,M., Sharma,J., Cheng,A., Leung,A., Liu,Y., Shih,W.M. and Yan,H. (2009) Multilayer DNA origami packed on a square lattice. *J. Am. Chem. Soc.*, **131**, 15903–15908.
6. Ke,Y., Sharma,J., Liu,M., Jahn,K., Liu,Y. and Yan,H. (2009) Scaffolded DNA origami of a DNA tetrahedron molecular container. *Nano Lett.*, **9**, 2445–2447.
7. Han,D., Pal,S., Nangreave,J., Deng,Z., Liu,Y. and Yan,H. (2011) DNA origami with complex curvatures in three-dimensional space. *Science*, **332**, 342–346.
8. Han,D., Pal,S., Yang,Y., Jiang,S., Nangreave,J., Liu,Y. and Yan,H. (2013) DNA gridiron nanostructures based on four-arm junctions. *Science*, **339**, 1412–1415.
9. Benson,E., Mohammed,A., Gardell,J., Masich,S., Czeizler,E., Orponen,P. and Hogberg,B. (2015) DNA rendering of polyhedral meshes at the nanoscale. *Nature*, **523**, 441–444.
10. Zhang,F., Jiang,S., Wu,S., Li,Y., Mao,C., Liu,Y. and Yan,H. (2015) Complex wireframe DNA origami nanostructures with multi-arm junction vertices. *Nat. Nano*, **10**, 779–784.
11. Matthies,M., Agarwal,N.P. and Schmidt,T.L. (2016) Design and synthesis of triangulated DNA origami trusses. *Nano Lett.*, **16**, 2108–2113.
12. Wei,B., Dai,M. and Yin,P. (2012) Complex shapes self-assembled from single-stranded DNA tiles. *Nature*, **485**, 623–626.
13. Ke,Y., Ong,L.L., Shih,W.M. and Yin,P. (2012) Three-dimensional structures self-assembled from DNA bricks. *Science*, **338**, 1177–1183.
14. Myhrvold,C., Dai,M., Silver,P.A. and Yin,P. (2013) Isothermal self-assembly of complex DNA structures under diverse biocompatible conditions. *Nano Lett.*, **13**, 4242–4248.
15. Wei,B., Dai,M., Myhrvold,C., Ke,Y., Jungmann,R. and Yin,P. (2013) Design space for complex DNA structures. *J. Am. Chem. Soc.*, **135**, 18080–18088.

16. Seeman,N.C. (1982) Nucleic acid junctions and lattices. *J. Theor. Biol.*, **99**, 237–247.
17. Mao,C., Sun,W. and Seeman,N.C. (1999) Designed two-dimensional DNA Holliday junction arrays visualized by atomic force microscopy. *J. Am. Chem. Soc.*, **121**, 5437–5443.
18. Yan,H., Park,S.H., Finkelstein,G., Reif,J.H. and LaBean,T.H. (2003) DNA-templated self-assembly of protein arrays and highly conductive nanowires. *Science*, **301**, 1882–1884.
19. He,Y., Chen,Y., Liu,H., Ribbe,A.E. and Mao,C. (2005) Self-assembly of hexagonal DNA two-dimensional (2D) arrays. *J. Am. Chem. Soc.*, **127**, 12202–12203.
20. He,Y., Tian,Y., Chen,Y., Deng,Z., Ribbe,A.E. and Mao,C. (2005) Sequence symmetry as a tool for designing DNA nanostructures. *Angew. Chem.*, **44**, 6694–6696.
21. Liu,Y., Ke,Y. and Yan,H. (2005) Self-assembly of symmetric finite-size DNA nanoarrays. *J. Am. Chem. Soc.*, **127**, 17140–17141.
22. He,Y., Tian,Y., Ribbe,A.E. and Mao,C. (2006) Highly connected two-dimensional crystals of DNA six-point-stars. *J. Am. Chem. Soc.*, **128**, 15978–15979.
23. Park,S.H., Pistol,C., Ahn,S.J., Reif,J.H., Lebeck,A.R., Dwyer,C. and LaBean,T.H. (2006) Finite-size, fully addressable DNA tile lattices formed by hierarchical assembly procedures. *Angew. Chem.*, **45**, 735–739.
24. Wang,X. and Seeman,N.C. (2007) Assembly and characterization of 8-arm and 12-arm DNA branched junctions. *J. Am. Chem. Soc.*, **129**, 8169–8176.
25. He,Y., Ye,T., Su,M., Zhang,C., Ribbe,A.E., Jiang,W. and Mao,C. (2008) Hierarchical self-assembly of DNA into symmetric supramolecular polyhedra. *Nature*, **452**, 198–201.
26. Malo,J., Mitchell,J.C. and Turberfield,A.J. (2009) A two-dimensional DNA array: the three-layer logpile. *J. Am. Chem. Soc.*, **131**, 13574–13575.
27. Sun,X., Hyeon Ko,S., Zhang,C., Ribbe,A.E. and Mao,C. (2009) Surface-mediated DNA self-assembly. *J. Am. Chem. Soc.*, **131**, 13248–13249.
28. Zhang,C., Ko,S.H., Su,M., Leng,Y., Ribbe,A.E., Jiang,W. and Mao,C. (2009) Symmetry controls the face geometry of DNA polyhedra. *J. Am. Chem. Soc.*, **131**, 1413–1415.
29. Zheng,J., Birktoft,J.J., Chen,Y., Wang,T., Sha,R., Constantinou,P.E., Ginell,S.L., Mao,C. and Seeman,N.C. (2009) From molecular to macroscopic via the rational design of a self-assembled 3D DNA crystal. *Nature*, **461**, 74–77.
30. He,Y., Su,M., Fang,P.A., Zhang,C., Ribbe,A.E., Jiang,W. and Mao,C. (2010) On the chirality of self-assembled DNA octahedra. *Angew. Chem.*, **49**, 748–751.
31. Ko,S.H., Su,M., Zhang,C., Ribbe,A.E., Jiang,W. and Mao,C. (2010) Synergistic self-assembly of RNA and DNA molecules. *Nat. Chem.*, **2**, 1050–1055.
32. Fu,T.J. and Seeman,N.C. (1993) DNA double-crossover molecules. *Biochemistry*, **32**, 3211–3220.
33. Winfree,E., Liu,F., Wenzler,L.A. and Seeman,N.C. (1998) Design and self-assembly of two-dimensional DNA crystals. *Nature*, **394**, 539–544.
34. LaBean,T.H., Yan,H., Kopatsch,J., Liu,F.R., Winfree,E., Reif,J.H. and Seeman,N.C. (2000) Construction, analysis, ligation, and self-assembly of DNA triple crossover complexes. *J. Am. Chem. Soc.*, **122**, 1848–1860.
35. Yan,H., Zhang,X., Shen,Z. and Seeman,N.C. (2002) A robust DNA mechanical device controlled by hybridization topology. *Nature*, **415**, 62–65.
36. Zhang,X., Yan,H., Shen,Z. and Seeman,N.C. (2002) Paranemic cohesion of topologically-closed DNA molecules. *J. Am. Chem. Soc.*, **124**, 12940–12941.
37. Mitchell,J.C., Harris,J.R., Malo,J., Bath,J. and Turberfield,A.J. (2004) Self-assembly of chiral DNA nanotubes. *J. Am. Chem. Soc.*, **126**, 16342–16343.
38. Rothemund,P.W., Papadakis,N. and Winfree,E. (2004) Algorithmic self-assembly of DNA Sierpinski triangles. *PLoS Biol.*, **2**, e424.
39. Barish,R.D., Rothemund,P.W. and Winfree,E. (2005) Two computational primitives for algorithmic self-assembly: copying and counting. *Nano Lett.*, **5**, 2586–2592.
40. Reishus,D., Shaw,B., Brun,Y., Chelyapov,N. and Adleman,L. (2005) Self-assembly of DNA double-double crossover complexes into high-density, doubly connected, planar structures. *J. Am. Chem. Soc.*, **127**, 17590–17591.
41. Ke,Y.G., Liu,Y., Zhang,J.P. and Yan,H. (2006) A study of DNA tube formation mechanisms using 4-, 8-, and 12-helix DNA nanostructures. *J. Am. Chem. Soc.*, **128**, 4414–4421.
42. Ding,B. and Seeman,N.C. (2006) Operation of a DNA robot arm inserted into a 2D DNA crystalline substrate. *Science*, **314**, 1583–1585.
43. Chelyapov,N., Brun,Y., Gopalkrishnan,M., Reishus,D., Shaw,B. and Adleman,L. (2004) DNA triangles and self-assembled hexagonal tilings. *J. Am. Chem. Soc.*, **126**, 13924–13925.
44. Chworos,A., Severcan,I., Koyfman,A.Y., Weinkam,P., Oroudjev,E., Hansma,H.G. and Jaeger,L. (2004) Building programmable jigsaw puzzles with RNA. *Science*, **306**, 2068–2072.
45. Ding,B., Sha,R. and Seeman,N.C. (2004) Pseudohexagonal 2D DNA crystals from double crossover cohesion. *J. Am. Chem. Soc.*, **126**, 10230–10231.
46. Liu,D., Wang,M., Deng,Z., Walulu,R. and Mao,C. (2004) Tensegrity: construction of rigid DNA triangles with flexible four-arm DNA junctions. *J. Am. Chem. Soc.*, **126**, 2324–2325.
47. Malo,J., Mitchell,J.C., Venien-Bryan,C., Harris,J.R., Wille,H., Sherratt,D.J. and Turberfield,A.J. (2005) Engineering a 2D protein-DNA crystal. *Angew. Chem.*, **44**, 3057–3061.
48. Mathieu,F., Liao,S., Kopatsch,J., Wang,T., Mao,C. and Seeman,N.C. (2005) Six-helix bundles designed from DNA. *Nano Lett.*, **5**, 661–665.
49. Park,S.H., Barish,R., Li,H.Y., Reif,J.H., Finkelstein,G., Yan,H. and LaBean,T.H. (2005) Three-helix bundle DNA tiles self-assemble into 2D lattice or 1D templates for silver nanowires. *Nano Lett.*, **5**, 693–696.
50. Wei,B. and Mi,Y. (2005) A new triple crossover triangle (TXT) motif for DNA self-assembly. *Biomacromolecules*, **6**, 2528–2532.
51. Liu,H., Chen,Y., He,Y., Ribbe,A.E. and Mao,C. (2006) Approaching the limit: can one DNA oligonucleotide assemble into large nanostructures? *Angew. Chem.*, **45**, 1942–1945.
52. Zheng,J.W., Constantinou,P.E., Micheel,C., Alivisatos,A.P., Kiehl,R.A. and Seeman,N.C. (2006) Two-dimensional nanoparticle arrays show the organizational power of robust DNA motifs. *Nano Lett.*, **6**, 1502–1504.
53. Kuzuya,A., Wang,R., Sha,R. and Seeman,N.C. (2007) Six-helix and eight-helix DNA nanotubes assembled from half-tubes. *Nano Lett.*, **7**, 1757–1763.
54. Zhang,C., He,Y., Chen,Y., Ribbe,A.E. and Mao,C.D. (2007) Aligning one-dimensional DNA duplexes into two-dimensional crystals. *J. Am. Chem. Soc.*, **129**, 14134–14135.
55. Aldaye,F.A., Lo,P.K., Karam,P., McLaughlin,C.K., Cosa,G. and Sleiman,H.F. (2009) Modular construction of DNA nanotubes of tunable geometry and single- or double-stranded character. *Nat. Nanotechnol.*, **4**, 349–352.
56. Hamada,S. and Murata,S. (2009) Substrate-assisted assembly of interconnected single-duplex DNA nanostructures. *Angew. Chem.*, **48**, 6820–6823.
57. Wang,R., Liu,W. and Seeman,N.C. (2009) Prototyping nanorod control: a DNA double helix sheathed within a DNA six-helix bundle. *Chem. Biol.*, **16**, 862–867.
58. Hansen,M.N., Zhang,A.M., Rangnekar,A., Bompiani,K.M., Carter,J.D., Gothelf,K.V. and LaBean,T.H. (2010) Weave tile architecture construction strategy for DNA nanotechnology. *J. Am. Chem. Soc.*, **132**, 14481–14486.
59. Wei,B., Wang,Z.Y. and Mi,Y.L. (2007) Uniquimer: software of de novo DNA sequence generation for DNA self-assembly—an introduction and the related applications in DNA self-assembly. *J. Comput. Theor. Nanosci.*, **4**, 133–141.
60. O'Neill,P., Rothemund,P.W., Kumar,A. and Fygenson,D.K. (2006) Sturdier DNA nanotubes via ligation. *Nano Lett.*, **6**, 1379–1383.
61. Barish,R.D., Schulman,R., Rothemund,P.W. and Winfree,E. (2009) An information-bearing seed for nucleating algorithmic self-assembly. *Proc. Natl. Acad. Sci. U.S.A.*, **106**, 6054–6059.
62. Hansma,H.G. and Laney,D.E. (1996) DNA binding to mica correlates with cationic radius: assay by atomic force microscopy. *Biophys. J.*, **70**, 1933–1939.
63. Sobczak,J.P., Martin,T.G., Gerling,T. and Dietz,H. (2012) Rapid folding of DNA into nanoscale shapes at constant temperature. *Science*, **338**, 1458–1461.

64. Ke,Y., Ong,L.L., Sun,W., Song,J., Dong,M., Shih,W.M. and Yin,P. (2014) DNA brick crystals with prescribed depths. *Nat. Chem.*, **6**, 994–1002.

65. Seeman,N.C. (2007) An overview of structural DNA nanotechnology. *Mol. Biotechnol.*, **37**, 246–257.

66. Seeman,N.C. (2010) Nanomaterials based on DNA. *Annu. Rev. Biochem.*, **79**, 65–87.

67. Simmel,S.S., Nickels,P.C. and Liedl,T. (2014) Wireframe and tensegrity DNA nanostructures. *Acc. Chem. Res.*, **47**, 1691–1699.

68. Lin,C., Liu,Y., Rinker,S. and Yan,H. (2006) DNA tile based self-assembly: building complex nanoarchitectures. *Chemphyschem*, **7**, 1641–1647.

69. Liu,W., Zhong,H., Wang,R. and Seeman,N.C. (2011) Crystalline two-dimensional DNA-origami arrays. *Angew. Chem.*, **50**, 264–267.

70. Reinhardt,A. and Frenkel,D. (2014) Numerical evidence for nucleated self-assembly of DNA brick structures. *Phys. Rev. Lett.*, **112**, 238103.